Check for updates

Zirconium metal–organic framework photocatalysis with TEMPO for blue light-powered aerobic sulfoxidation†

Bing Zeng, Yuexin Wang, Kanghui Xiong, Keke Zhang, Siyu Zhang and Xianjun Lang [ID] *

A zirconium metal–organic framework (MOF), NU-1003, along with TEMPO (2,2,6,6-tetramethylpiperidine-*N*-oxyl), is constructed as a system of cooperative photocatalysis for blue light-powered aerobic sulfoxidation. The incorporation of 4 mol% of TEMPO enhances the hole transfer and thereby aerobic sulfoxidation by NU-1003 photocatalysis, demonstrating the pivotal role of a redox mediator in transforming an established MOF.

Given the growing concerns about energy and environmental issues, there is an increasing demand for developing and utilizing clean and sustainable energy.[1] In this regard, abundant and inexhaustible solar energy is one of the most attractive sources of alternative energy.[2] Nevertheless, solar energy is challenging to be utilized directly due to low density and sporadic availability.[3] Inspired by natural photosynthesis, semiconductor photocatalysis has been extensively studied to convert solar energy into chemical energy.[4] Despite the significant potential of photocatalysis, its efficiency is limited by factors such as active sites, charge carrier recombination, and light absorption. As such, the design of highly efficient systems of semiconductor photocatalysis is imperative.

As semiconductor-like materials, metal–organic frameworks (MOFs) are a class of porous crystalline materials composed of metal–oxo clusters and organic ligands. Due to the tailored structures, large specific surface area, and high porosity, MOFs have been recognized as an ideal platform for photocatalysis.[5] However, the low conductivity and poor stability hinder their widespread application.[6] Significant efforts have been made to solve these issues. For instance, zirconium (Zr) MOFs exhibit remarkable mechanical and chemical stability in practical applications, attributed to the strong ionic interaction between carboxylate oxygen atoms and Zr(IV) clusters.[7] Recently, a Zr

MOF BUT-73 with the 6,6′,6″,6‴-(pyrene-1,3,6,8-tetrayl)tetrakis-(2-naphthoic acid) (PTNA) ligand has been reported with excellent stability.[8] By the same token, Zr MOF NU-1003, with sizeable specific surface area and high porosity, has been primarily explored for adsorption and catalysis.[9,10] Moreover, these Zr MOFs are promising to make a splash in semiconductor photocatalysis.

Generally, the efficiency of MOF photocatalysis is influenced by the rapid recombination of electrons and holes, which in turn cannot power redox reactions.[11,12] An effective strategy to regulate the efficiency of photogenerated charge carriers is urgently needed for MOF photocatalysis. To this end, a simple and efficient strategy is the incorporation of a redox mediator TEMPO (2,2,6,6-tetramethylpiperidine-*N*-oxyl) to facilitate hole transfers, thereby improving visible light-powered redox reactions.[13–15] In this study, a MOF, NU-1003, is synthesized by a solvothermal reaction of Zr(IV) oxychloride octahydrate ($ZrOCl_2 \cdot 8H_2O$) and the PTNA ligand in *N,N*-dimethylformamide (DMF) (Fig. 1). Intriguingly, the efficiency of NU-1003 photocatalysis is improved by the incorporation of a catalytic amount of TEMPO. Specifically, TEMPO facilitates efficient hole transfer of the photoexcited NU-1003, resulting in efficient blue light-powered aerobic sulfoxidation with superoxide ($O_2^{\bullet-}$) as the main reactive oxygen species (ROS).
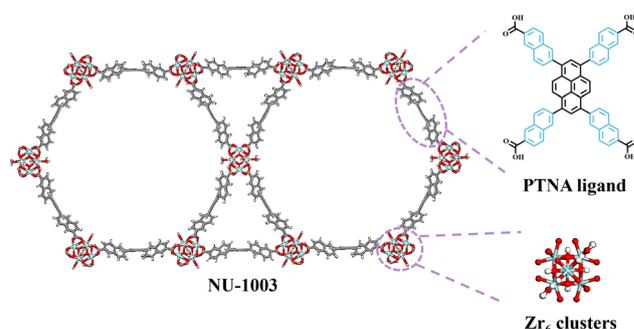
Hubei Key Lab on Organic and Polymeric Optoelectronic Materials, College of Chemistry and Molecular Sciences, Wuhan University, Wuhan 430072, China.
E-mail: xianjunlang@whu.edu.cn

Fig. 1 Schematic representation of NU-1003.

The crystalline structure of NU-1003 was confirmed through powder X-ray diffraction (PXRD). The experimental data matched well with the simulated data in the PXRD patterns (Fig. 2a). The successful synthesis of NU-1003 was further confirmed by comparing the PXRD pattern of the PTNA ligand (Fig. S1, ESI†). The nitrogen (N_2) sorption isotherms for NU-1003 at 77 K (Fig. 2b) exhibited two pronounced increases at higher partial pressures, corresponding to the filling of the microporous triangular channels and the mesoporous hexagonal channels, respectively. The Brunauer–Emmett–Teller (BET) specific surface area was determined to be 325 $m^2\ g^{-1}$ and the pore size distribution, calculated using a non-local density functional theory (DFT) model, revealed two major peaks at 1.2 nm and 3.4 nm for NU-1003. The scanning electron microscopy (SEM) image indicates that NU-1003 possessed a regular rod-like morphology (Fig. 2c). High-resolution transmission electron microscopy (HRTEM) and fast Fourier transform (FFT) analysis also confirmed the crystalline nature of NU-1003 (Fig. 2d), which is consistent with the PXRD data. The thermogravimetric analysis (TGA) curve was acquired to evaluate the thermal stability of NU-1003 under an N_2 atmosphere (Fig. S2, ESI†). There was a thermal weight loss of 10% occurring above 300 °C.

Next, the solid-state UV-visible spectroscopy revealed that NU-1003 possessed a significant and broad visible light absorption band ranging from 300 to 600 nm (Fig. 3a). The corresponding bandgap, determined from the Tauc plot (Fig. 3b), was calculated to be 2.52 eV. The flat band potential (E_{fb}), which approximates the position of the lowest unoccupied molecular orbital (LUMO) potential, was estimated to be −0.90 V $vs.$ Ag/AgCl, based on the Mott–Schottky plots (Fig. S3a, ESI†). In comparison to the reduction potential of $O_2/O_2^{\bullet-}$ (−0.46 V $vs.$ Ag/AgCl),[16] the more negative LUMO potential suggests that NU-1003 can initiate the generation of the ROS $O_2^{\bullet-}$. Consequently, the highest occupied molecular orbital (HOMO) potential was determined to be 1.62 V $vs.$ Ag/AgCl (Fig. S3b, ESI†). Optoelectronic measurements were then used to investigate the charge separation and transfer properties of NU-1003. Notably, when a
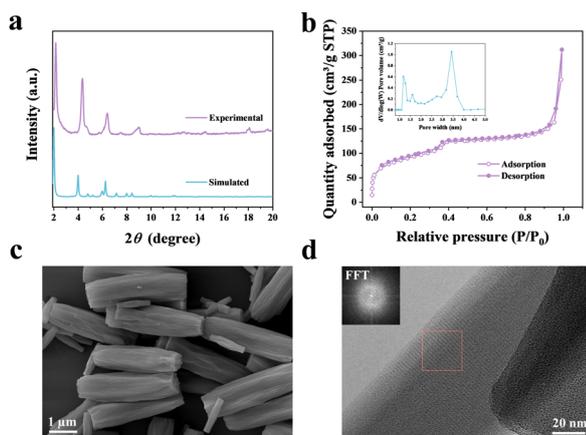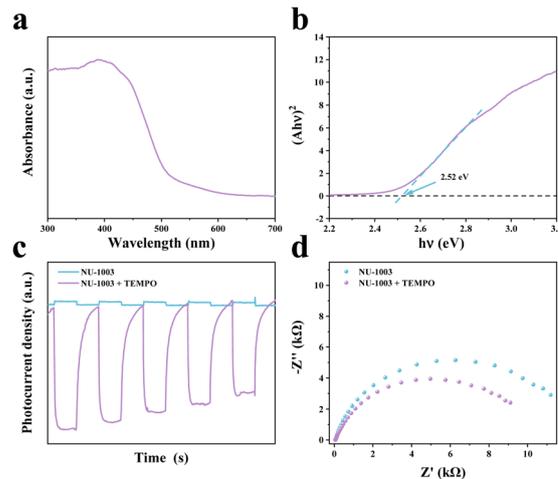

Fig. 3 (a) Solid-state UV-visible spectrum and (b) the corresponding Tauc plot of NU-1003. The transient photocurrent densities (c) and EIS Nyquist plots (d) of NU-1003 with or without TEMPO.

tiny amount of TEMPO was incorporated into the 0.1 M ammonium hexafluorophosphate (NH_4PF_6) acetonitrile electrolyte, NU-1003 with TEMPO exhibited a higher transient photocurrent density than NU-1003 without TEMPO (Fig. 3c). The resistance of photogenerated charge transfer was assessed using the arc radius of electrochemical impedance spectroscopy (EIS). As shown in Fig. 3d, the EIS Nyquist plot of NU-1003 with TEMPO revealed a smaller arc radius than that of NU-1003 without TEMPO, indicating lower charge transfer resistance. These observations demonstrate the superiority of NU-1003 with TEMPO in improving optoelectronic efficiency.

The green synthesis of organic sulfoxides, which are crucial intermediates in pharmaceutical industries, has garnered significant interest in recent years.[17] Among them, the aerobic sulfoxidation by photocatalysis, utilizing visible light and O_2, is one of the most sustainable approaches.[11] To date, NU-1003 has not yet been applied in visible light photocatalysis. Additionally, TEMPO can facilitate hole transfer, thereby enhancing the efficiency of MOFs. The efficiency of NU-1003 photocatalysis with TEMPO was evaluated through a model reaction of the oxidation of organic sulfide to sulfoxide under blue LED irradiation. Initially, kinetic tests were conducted (Fig. 4a). As expected, with sufficient irradiation time, the incorporation of a catalytic amount of TEMPO furnished superior efficiency for blue light-powered aerobic sulfoxidation compared to pristine NU-1003 photocatalysis. Furthermore, aerobic sulfoxidation by NU-1003 photocatalysis exhibited zero-order reaction, with or without the incorporation of 4 mol% of TEMPO. Moreover, the conversion of methyl phenyl sulfide increased gradually with the increasing amount of TEMPO loaded until it plateaued and then somewhat rebounded with further loading of TEMPO, in which 4 mol% of TEMPO demonstrated the highest efficiency of NU-1003 photocatalysis (Fig. 4b). This was indicative of a cooperative effect between NU-1003 and TEMPO. To further explore the versatility of cooperative photocatalysis, methyl phenyl sulfides with different substituent groups were subjected to the identical
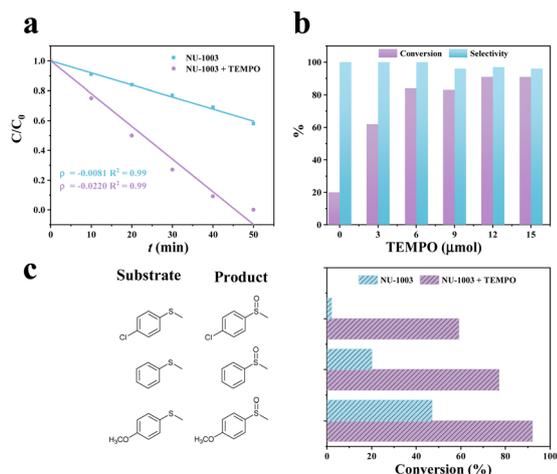

Fig. 2 (a) PXRD patterns of experimental and simulated data of NU-1003. (b) The N_2 sorption isotherms (inset: pore size distribution) of NU-1003 at 77 K. The SEM image (c) and HRTEM image (d) of NU-1003.

Fig. 4 (a) Kinetic curves of blue light-powered aerobic oxidation of methyl phenyl sulfide by NU-1003 photocatalysis with or without TEMPO. (b) The change in TEMPO concentration for aerobic sulfoxidation. (c) The effect of 4 mol% TEMPO for aerobic sulfoxidation by NU-1003 photo-catalysis. Standard reaction conditions: NU-1003 (5 mg), methyl phenyl sulfide (0.3 mmol), TEMPO (12 μmol, 4 mol%), blue LEDs, solvent (CF_3CH_2OH, 1 mL), air (1 atm), 1 h.

conditions (Fig. 4c). The incorporation of TEMPO significantly improved the efficiency of NU-1003 photocatalysis. Moreover, the reaction proceeded more smoothly with sulfide containing an electron-donating group, like methyl *p*-methoxyphenyl sulfide, as opposed to sulfide with an electron-withdrawing group, like methyl *p*-chlorophenyl sulfide. Therefore, NU-1003 photocatalysis and TEMPO present an effective strategy for the aerobic oxidation of sulfides to sulfoxides under blue LED irradiation.

Meanwhile, the effects of solvents and irradiation wavelengths of visible light on the aerobic oxidation of methyl phenyl sulfide to methyl phenyl sulfoxide were investigated to determine the optimal reaction conditions. According to Table S1 (ESI†), the solvent significantly influenced the conversion of methyl phenyl sulfide. Trifluoroethanol (CF_3CH_2OH), a protic solvent, achieved the highest conversion of 91%, while an aprotic solvent acetonitrile (CH_3CN) exhibited a much lower conversion of 3%. The difference likely results from a proton exchange process, as CF_3CH_2OH demonstrates superior proton-donating capacity. Additionally, the aerobic oxidation of methyl phenyl sulfide was achieved by NU-1003 photocatalysis with 4 mol% of TEMPO under visible light LED irradiation with wavelengths shorter than 590 nm (Fig. S4, ESI†), consistent with the solid-state UV-visible spectrum. The highest conversion was observed under 460 nm blue LED irradiation (Fig. S5, ESI†), making it the preferred light source for subsequent experiments. After four cycles, no significant decrease in photocatalytic efficiency was observed for the conversions of methyl phenyl sulfide and selectivities of methyl phenyl sulfoxide (Fig. S6, ESI†), indicating the exceptional durability of NU-1003. Additionally, the nearly unchanged SEM image and Fourier transform infrared (FTIR) spectra after four cycles (Fig. S7 and S8, ESI†) further demonstrated the structural integrity and chemical stability of NU-1003.

With the optimal conditions for NU-1003 photocatalysis with 4 mol% of TEMPO, the substrate scope for aerobic sulfoxidation was expanded to include various organic sulfides with electron-withdrawing and electron-donating substituent groups (Table S2, ESI†). Remarkably, 91% conversion of methyl phenyl sulfide to methyl phenyl sulfoxide was achieved by NU-1003 photocatalysis with 4 mol% of TEMPO in 1 h (Table S2, entry 1, ESI†). Electron-donating groups such as $-CH_3$ and $-OCH_3$ were introduced at the *para*-position of the phenyl ring in methyl phenyl sulfide (Table S2, entries 2 and 3, ESI†). Encouragingly, the corresponding sulfoxides were produced smoothly, achieving conversions of 90% and 97% in 0.8 h, respectively. When electron-withdrawing groups such as $-F$, $-Cl$, $-Br$, and $-I$ were introduced, the corresponding sulfoxides were obtained in conversions of 92%, 81%, 92% and 97%, respectively, over 1.8 h (Table S2, entries 6–11, ESI†). The electronic effects significantly influenced conversion. Moreover, sulfides with substituent groups on the *meta*- and *ortho*-positions of the phenyl ring were also efficiently converted, albeit with longer reaction time (Table S2, entries 4, 5 and 8, 9, ESI†). When the methyl group in methyl phenyl sulfide was replaced with an ethyl or phenyl group, the conversions decreased (Table S2, entries 12 and 13, ESI†). Additionally, aliphatic sulfide was converted to the corresponding sulfoxide with shorter reaction time for a comparable conversion (Table S2, entry 14, ESI†).

To elucidate the underlying mechanism of aerobic sulfoxidation by NU-1003 photocatalysis with TEMPO, various quenching experiments and *in situ* electron paramagnetic resonance (EPR) spectroscopic studies were conducted to verify the ROS. Notably, cooperative photocatalysis of NU-1003 with TEMPO exhibited excellent efficiency, achieving a high conversion of 91% of methyl phenyl sulfide at 1 h under the standard reaction conditions (Fig. 5a). However, the reaction did not proceed under an N_2 atmosphere, indicating that O_2 is essential. After adding a typical $O_2^{\bullet-}$ scavenger, *p*-benzoquinone (*p*-BQ), no detectable sulfoxide product was observed. When CF_3CD_2OD was used as a solvent to extend the lifetime of singlet oxygen ($^1O_2$), the conversion did not improve, which nearly excludes the involvement of $^1O_2$. The main ROS involved in the aerobic sulfoxidation by NU-1003 photocatalysis with TEMPO was $O_2^{\bullet-}$. After adding 1 equivalent (equiv.) of $AgNO_3$ (electron scavenger) and 3 equiv. of HCOOH (hole scavenger), the conversion of methyl phenyl sulfide sharply decreased, suggesting that the photogenerated electron and hole were essential in executing the reaction. Impressively, the results are quite consistent with the EPR results. No characteristic electron signal peak was observed in the dark condition. Intriguingly, when O_2 was introduced for 2 min, the electron signal degraded significantly, demonstrating that O_2 was likely reduced to $O_2^{\bullet-}$ by electrons. 5,5-Dimethyl-pyrroline-*N*-oxide (DMPO) was employed as an $O_2^{\bullet-}$ trapping agent. NU-1003 was added to DMPO and tested. A distinct and characteristic signal of $O_2^{\bullet-}$ was observed during the reaction (Fig. 5c), with the signal strengthed gradually increasing as the irradiation time increased. It is shown that the production of ROS on the aerobic sulfoxidation was $O_2^{\bullet-}$, in accordance with the quenching results. After that, three characteristic signals provided direct
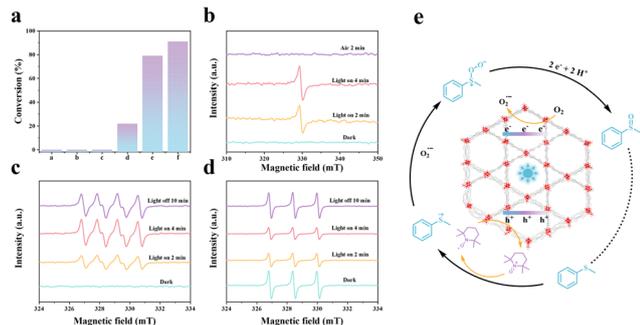
Fig. 5 (a) Quenching results for aerobic sulfoxidation by NU-1003 photocatalysis with TEMPO. a, N$_2$ atmosphere; b, *p*-BQ (0.2 equiv.); c, AgNO$_3$ (1 equiv.); d, HCOOH (3 equiv.); e, solvent (CF$_3$CD$_2$OD, 1 mL); f, standard reaction conditions: NU-1003 (5 mg), methyl phenyl sulfide (0.3 mmol), TEMPO (12 μmol, 4 mol%), blue LEDs, solvent (CF$_3$CH$_2$OH, 1 mL), 1 h. The EPR spectra of (b) electron; (c) DMPO−O$_2$$^{\bullet-}$; and (d) TEMPO. (e) A possible mechanism for the blue light-powered aerobic sulfoxidation by NU-1003 photocatalysis with TEMPO.

evidence of the transmutation of TEMPO (Fig. 5d),[18] which gradually weakened as extending the irradiation time. This indicates that TEMPO was involved in the aerobic sulfoxidation. In particular, the signal for TEMPO restored after turning off the light irradiation, illustrating a closed redox cycle for TEMPO in the reaction.

Based on the findings, a possible mechanism for blue light-powered aerobic sulfoxidation by NU-1003 photocatalysis with TEMPO is proposed (Fig. 5d). Under blue LED irradiation, charge separation occurs in NU-1003, resulting in the generation of electrons (e$^-$) and holes (h$^+$). On the one hand, e$^-$ transfers to O$_2$, forming O$_2$$^{\bullet-}$. Conversely, h$^+$ remaining on NU-1003 oxidizes TEMPO to TEMPO$^+$, which subsequently interacts with methyl phenyl sulfide to produce a radical cation. Simultaneously, TEMPO$^+$ is reduced to TEMPO, participating in the next redox cycle. O$_2$$^{\bullet-}$ then nucleophilically attacks the methyl phenyl sulfide radical cation, transforming it into persulfoxide. Ultimately, protons and electrons from the reaction medium CF$_3$CH$_2$OH facilitate the conversion of methyl phenyl persulfoxide into the ultimate product, methyl phenyl sulfoxide.

In summary, NU-1003 and TEMPO acted as a system of cooperative photocatalysis for blue light-powered aerobic sulfoxidation with excellent selectivities at high conversions. Optoelectronic measurements indicated that TEMPO enhanced hole transfer during sulfoxidation. Specifically, NU-1003 marginally impelled the conversion of organic sulfides. In contrast, the incorporation of 4 mol% of TEMPO significantly improved the efficiency of NU-1003 photocatalysis, with a high conversion of organic sulfides. Notably, the system of cooperative photocatalysis facilitated the generation of sulfoxide *via* an electron transfer pathway. More importantly, TEMPO enhances the hole

transfer of MOF photocatalysis in facilitating selective organic transformations, providing new insights for solar energy utilizations.

Data availability

The data supporting this article have been included as part of the ESI.†

Conflicts of interest

There are no conflicts to declare.

Notes and references

1 X. S. Hu, D. X. Zuo, S. R. Cheng, S. H. Chen, Y. Liu, W. Z. Bao, S. L. Deng, S. J. Harris and J. Y. Wan, *Chem. Soc. Rev.*, 2023, **52**, 1103–1128.
2 J. Q. Lv, J. F. Xie, A. G. A. Mohamed, X. Zhang, Y. Y. Feng, L. Jiao, E. B. Zhou, D. Q. Yuan and Y. B. Wang, *Nat. Rev. Chem.*, 2023, **7**, 91–105.
3 X. D. Sun, S. Y. Jiang, H. W. Huang, H. Li, B. H. Jia and T. Y. Ma, *Angew. Chem., Int. Ed.*, 2022, **61**, e202204880.
4 J. D. Xiao and H. L. Jiang, *Acc. Chem. Res.*, 2019, **52**, 356–366.
5 H. G. Jin, P. C. Zhao, Y. Y. Qian, J. D. Xiao, Z. S. Chao and H. L. Jiang, *Chem. Soc. Rev.*, 2024, **53**, 9378–9418.
6 Y. P. Zhang, J. X. Xu, J. Zhou and L. Wang, *Chin. J. Catal.*, 2022, **43**, 971–1000.
7 K. Wu, X. Y. Liu, P. W. Cheng, Y. L. Huang, J. Zheng, M. Xie, W. G. Lu and D. Li, *J. Am. Chem. Soc.*, 2023, **145**, 18931–18938.
8 C. Dong, J. Q. Bai, X. L. Lv, W. Wu, J. Lv and J. R. Li, *Inorg. Chem.*, 2019, **58**, 15909–15916.
9 H. Y. Chen, Z. J. Chen, O. K. Farha and R. Q. Snurr, *ACS Sustainable Chem. Eng.*, 2019, **7**, 18242–18246.
10 P. Li, S. Y. Moon, M. A. Guelta, L. Lin, D. A. Gómez-Gualdrón, R. Q. Snurr, S. P. Harvey, J. T. Hupp and O. K. Farha, *ACS Nano*, 2016, **10**, 9174–9182.
11 H. N. Li, Y. Yang, X. Jing, C. He and C. Y. Duan, *Chem. Commun.*, 2023, **59**, 11220–11223.
12 W. J. Xu, B. X. Huang, G. L. Li, F. Yang, W. Lin, J. X. Gu, H. G. Deng, Z. G. Gu and H. G. Jin, *ACS Catal.*, 2023, **13**, 5723–5732.
13 B. Zeng, W. L. Sheng, F. W. Huang, K. K. Zhang, K. H. Xiong and X. J. Lang, *Chem. Eng. J.*, 2023, **474**, 145559.
14 B. Zeng, F. W. Huang, Y. X. Wang, K. H. Xiong and X. J. Lang, *Chin. J. Catal.*, 2024, **58**, 226–236.
15 F. W. Huang, F. L. Zhang, Y. X. Wang and X. J. Lang, *Trends Chem.*, 2024, **6**, 115–127.
16 D. Ma, P. Li, X. Y. Duan, J. Z. Li, P. P. Shao, Z. L. Lang, L. X. Bao, Y. Y. Zhang, Z. G. Lin and B. Wang, *Angew. Chem., Int. Ed.*, 2020, **59**, 3905–3909.
17 S. Suleman, Y. Zhang, Y. Y. Qian, J. W. Zhang, Z. Y. Lin, O. Metin, Z. Meng and H. L. Jiang, *Angew. Chem. Int. Ed.*, 2024, **63**, 202314988.
18 X. W. Lan, Q. Li, Y. Z. Zhang, Q. Li, L. Ricardez-Sandoval and G. Y. Bai, *Appl. Catal., B*, 2020, **277**, 119274.